Use of alkali activated high-calcium fly ash binder for kaolin clay soil stabilisation: Physicochemical evolution

Elodie Coudert[a,b,c], Michael Paris[a], Dimitri Deneele[a,d*], Giacomo Russo[b], Alessandro Tarantino[c]

[a] Institut des Matériaux Jean Rouxel (IMN), Université de Nantes, CNRS, 2 rue de la Houssinière, BP 32229, 44322 Nantes Cedex 3, France

[b] Department of Civil and Mechanical Engineering, University of Cassino and Southern Lazio, Via Gaetano di Biasio, 43, 03043 Cassino, FR, Italy

[c] Department of Civil and Environmental Engineering, University of Strathclyde, 75 Montrose Street, Glasgow, Scotland, G1 1XJ, United Kingdom

[d] IFSTTAR, GERS, EE, F-44344 Bouguenais, France.

*Corresponding author

Phone : + 33 2 40 84 58 02

Fax: + 33 2 40 58 57 77

E-mail: Dimitri.Deneele@ifsttar.fr

Abstract

This study addresses the use of alkali activated high-calcium fly ash-based binder to improve engineering characteristics of soft clay-rich soils as an alternative to common stabilisers. The physico-chemical reaction sequence has been investigated by considering the binder alone and the binder mixed with kaolin. An insight into the reactivity evidenced that calcium-containing phases derived from high-calcium fly ash represent the reactive phases and, hence, pozzolanic activity is the dominant process. New compounds are

formed, thenardite Na_2SO_4 and an amorphous silicate consisting of chains combined with calcium probably incorporating three-dimensional four-fold aluminium environments.

Keywords

Soil stabilisation; Alkali activated material; Kaolin; High-calcium fly ash

1. Introduction

Soft clay-rich soils are frequently encountered in construction sites. Their poor mechanical performance represents a critical issue in engineering projects. These soils cannot be directly used as earthfill materials and may cause excessive settlements of foundation structures. To improve their engineering characteristics chemical stabilisation involving the addition of a binder to the soil has been widely practiced. The commonly used stabilisers are Ordinary Portland Cement and lime whose stabilisation mechanisms have been widely reported [1-7]. Nevertheless, a major issue with those conventional stabilisers is a very significant environmental penalty due to high carbon dioxide emissions and energy intensive processes.

In the low carbon agenda, the development of novel technologies that are both cost- and carbon-efficient is of prime importance, particularly in the construction sector for which cement production contributes to at least 5–8% of global carbon dioxide emissions [8]. As an alternative, industrial by-products such as high-calcium fly ash, rice husk ash, and silica fume have been successfully mixed as cementing additives to soft soils resulting in environmental and economic benefits [9-15].

Another alternative gaining attention is the use of Alkali Activated Materials as a viable sustainable binder whose often-claimed advantage is a much lower CO_2 emission process compared to traditional Portland cement. Works on alkali activated soils are recent and aim to stabilise different types of soil from clayey soil [16-17], sandy clay [18], Lateritic soils [19] marl, marlstone [20], silty sand [21], road aggregates [22] to mixed soil synthesised in laboratory [23-24]. The overall work shows the potential of alkaline activation for soil improvement, and this for different designed applications i.e. in deep soft soil [18], at shallow depth [24] or in rammed earth construction [25].

53 Alkali Activated Materials are defined as any binder system derived by the reaction of an
54 alkali metal source (usually alkali hydroxide and alkali silicate solutions) with a solid
55 aluminosilicate powder (commonly metakaolin, fly ash, blast furnace slag or natural
56 pozzolan) [26-27]. It gives a hardened material at room temperature with mechanical
57 properties potentially suitable for Portland cement replacement.
58 The type of aluminosilicate material needed in the alkali activation process varies as well.
59 In fact, most of the studies were conducted on the use of fly ash [16-18; 20-21;23-25; 28-
60 29]. Nevertheless, Zhang et al. [24] also examined the feasibility of metakaolin based
61 alkali activated soil, and some other studies established on slag based alkali activated soil
62 are as well existing [16, 17, 23].
63 As stabilisation using alkaline activation is a recent research area, studies about the
64 understanding of the physicochemical reactivity of such systems have received little
65 attention so far [17] . Yet, the molecular structure and the chemical composition of the
66 alkali activated binders is essential to properly assess the resulting strength and durability
67 of the final material.
68 This work focuses on the use of calcium-rich high-calcium fly ash from coal combustion
69 activated by sodium-based alkaline solution as a binder for clay kaolin stabilisation. High-
70 calcium fly ash was selected in the context of resource-saving being an industrial waste.
71 Kaolin was selected as a model soil to represent a wide class of clays encountered in
72 engineering projects.
73 The study was designed in three stages. An initial stage consisted in the investigation of
74 the reactivity of the alkali activated high-calcium fly ash binder by itself, including (i)
75 which phases are present and which phases are accessible during alkaline activation, (ii)
76 which compounds are subsequently formed, and (iii) reactivity timescale. A second stage

77 focused on the interaction of the high-calcium fly ash-based binder with the kaolin clay
78 to understand how the presence of kaolin modifies the reactivity of the system. Kaolinite
79 is generally unreactive to alkali attack at ambient temperature. However, the addition of
80 clay may affect chemical reactions as occurs in clay-cement mix [30].
81 Finally, the physicochemical evolution occurring in the alkali activated high-calcium fly
82 ash is compared with one occurring in the same kaolin stabilised by i) lime or ii) a mix of
83 lime and the same high-calcium fly ash used in this experimental programme. This is
84 aimed at assessing the potential benefit of high-calcium fly ash-based binder compared
85 to the more traditional lime.
86

2. Material and methods

2.1 Materials

A Polish high-calcium fly ash derived from hard coal and coal slime combustion in fluidised bed boiler was used. Its chemical analysis is given in Table 1, and consists primarily of SiO_2, Al_2O_3 and CaO. The high-calcium fly ash contains, approximately, 52% of particles sized lower than 45 µm and 41% lower than 10 µm.

Speswhite kaolin provided by Imerys Minerals UK, and whose chemical composition is given in Table 1 was used. It is mainly constituted of kaolinite (95%) and secondarily of muscovite (4%) [3]. The kaolin contains, approximately, 100 % of particles sized lower than 10 µm and 80 % lower than 2 µm.

A unique alkaline solution was used: a sodium silicate with a mass ratio SiO_2/Na_2O of 1.7 and a dry mass percentage of 44%; supplied by Woellner group and named GEOSIL 34417.

Table 1

Chemical composition (wt. %) of raw fly ash and kaolin.

	SiO_2	Al_2O_3	Fe_2O_3	CaO	CaO_{free}[a]	MgO	SO_3	Na_2O	K_2O	H_2O	L.o.I.
Fly ash	39.4	19.8	7.4	18.6	5.2	1.8	4.1	2.0	1.8	0.0	1.7[b]
Kaolin	49.2	34.5	1.2	0.0	0.0	0.2	0.0	0.1	1.7	13.1	12.0[c]

[a] Free calcium oxide content, [b] from [3], [c] from [33]

2.2 Sample preparation

Sample preparation consisted in (i) mix of liquid sources ie. silicate and water (ii) mix of aluminosilicate powders ie. high-calcium fly ash and kaolin in the case of soil-source sample (iii) mix of (i) and (ii) previously prepared.

Three types of mixes were studied and named F100, KF50 and KF20. F100 is the high-calcium fly ash based alkali activated binder. It corresponds to a solid phase made of

high-calcium fly ash only, whereas KF50 and KF20 are the alkali activated soils. KF50 corresponding to a solid phase made of 50% of high-calcium fly ash and 50% of kaolin in mass, and KF20 corresponding to a solid phase made of 20% of high-calcium fly ash and 80% of kaolin. List of samples is summarized up in Table 2.

To ensure a good workability, the amount of added water with respect to the solid mass (eg. mass of kaolin and high-calcium fly ash) was fixed to 50% for all the samples. Additionally, the mass ratio of alkaline solution to high-calcium fly ash was fixed to 50% for all the samples, giving the initial molar ratios (considering that kaolin is unreactive): Si/Al = 2.0, Si/Na = 3.5 and Al/Na = 1.8. The Al/Na ratio was not fixed to one because of the presence of calcium ions in high quantity in our system playing a role of charge compensation as well as sodium.

The paste obtained was poured in closed plastic molds and cured at room temperature (20 °C). Samples were finally demoulded and freeze dried at curing times of 1, 3, 7 or 28 days.

Table 2

Samples composition wt. %.

Sample	Fly ash	Kaolin	Water	Alkaline solution
F100	50	0	25	25
KF50	28.6	28.6	28.6	14.3
KF20	12.5	50	31.3	6.3

2.3 Methods

A variety of characterisation techniques were complementary used to probe the mineralogical, structural and microstructural sample characteristics.

X-ray diffractograms of powdered samples were obtained with a Bruker D8 Advance diffractometer, using CuKα radiation generated at 40 mA and 40kV. Specimens were step-scanned from 2 to 60° 2θ at 0.017° 2θ steps integrated at the rate of 1s/step.

Derivative thermogravimetric curves were obtained on a Netzsch STA 449F3 Jupiter thermal analyser. The samples were heated from 20–1000 °C at a rate of 10 °C/min under argon atmosphere.

FTIR spectra were obtained on an FTIR Bruker Vertex 70 spectrometer. Specimens were prepared by mixing 30 mg of sample in 270 mg of KBr. Spectral analysis was performed over the range 4000–400 cm^{-1} at a resolution of 4 cm^{-1}.

Solid-state ^{29}Si NMR spectroscopy was performed using a Bruker Avance III 300 MHz (7 T) spectrometer and 7 mm MAS probe. ^{29}Si MAS spectra were acquired with a single $\pi/2$ pulse excitation of 5.5 μs and ^{1}H decoupling. The repetition times were 2 s, 120 s and 30 s for the raw high-calcium fly ash, the raw kaolin and all the activated samples, respectively. For all ^{29}Si spectra, MAS spinning rate was set to 5 kHz. Solid-state ^{27}Al NMR spectroscopy was performed using a Bruker Avance III 500 MHz (11.7 T) spectrometer and 2.5 mm MAS probe. ^{27}Al MAS spectra were acquired with a single pulse excitation of $\pi/12$ pulse of 3.3 μs and ^{1}H decoupling. Repetition time was set to 1 s and MAS spinning rate to 30 kHz. Spectra were referenced against TMS (tetramethylsilane) for ^{29}Si and an $Al(NO_3)_3$ aqueous solution for ^{27}Al. Lastly, attention should be drawn to the fact that iron initially present in the high-calcium fly ash renders the interpretation more complex, notably spectra from different mixes cannot be quantitatively compared.

Finally, samples were studied by SEM from polished section. Freeze-dried samples were impregnated under a vacuum with an acrylic resin (LR White). The polymerisation of the

154 resin was performed in an oven at 60°C over 48 h. The samples were then polished with
155 diamond powder and coated with carbon before the observation. The observations were
156 done with a HITACHI SU5000 scanning electron microscope equipped with an energy-
157 dispersive X-ray analyser (Quantax microanalyser system composed of X-Flash® SDD
158 detector and the Esprit software). The microscope was operated at an accelerating voltage
159 of 20 kV and working distances of 10 mm.

160 **3. Results and discussion**

161 The first section of results presents the physico-chemical evolution of the binder alone
162 without the addition of kaolin. The second part focuses on the description of the soil
163 source material mixed with binder. To end with, the system investigated in this study is
164 compared with lime-based systems already described in the literature.

165 *3.1 Alkali activated high-calcium fly ash binder*

166 *3.1.1 X-ray diffraction (XRD)*

167 Results obtained by XRD show that the original high-calcium fly ash is constituted of a
168 vitreous phase (hump between 17°2θ and 38°2θ), and crystalline phases which include
169 calcium-containing minerals: anhydrite $CaSO_4$, calcite $CaCO_3$ and portlandite $Ca(OH)_2$,
170 and other minerals: quartz SiO_2, feldspar $(K,Na,Ca)(Si,Al)_4O_8$, hematite Fe_2O_3 and
171 muscovite $(Si_3Al)O_{10}(Al_2)(OH)_2K$ (Fig. 1).

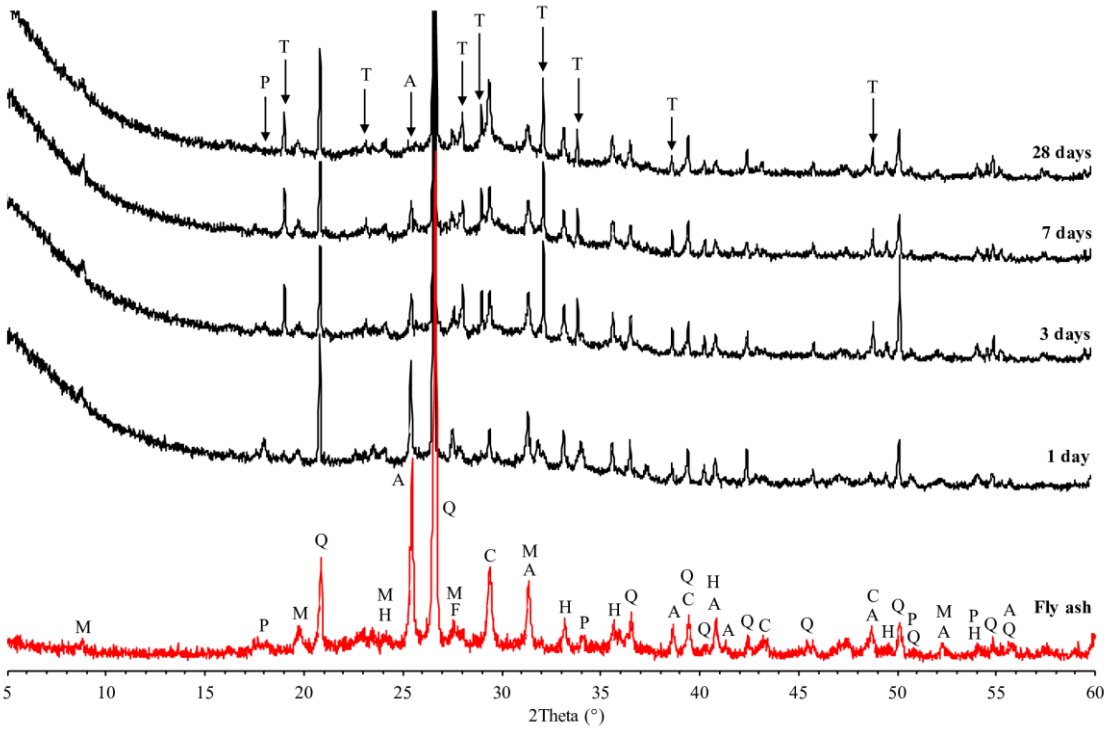

Fig. 1. XRD of raw fly ash and fly ash based alkali activated material F100 as a function of curing time; A=anhydrite; C=calcite; F=feldspar; H=hematite; M=muscovite; P=portlandite; Q=quartz; T=thenardite.

Fig. 1 also shows XRD patterns of the alkali activated high-calcium fly ash as a function of curing time. Regarding the crystalline phases, anhydrite $CaSO_4$ and portlandite $Ca(OH)_2$ are consumed as a function of time. In addition, thenardite Na_2SO_4 starts forming at 3 days. Its formation can be explained by the release of sulphate anions from anhydrite dissolution, and its subsequent combination with sodium issued from the alkaline solution.

3.1.2 Derivative thermogravimetric analysis (DTG)

Fig. 2 shows derivative thermogravimetric analyses of the original high-calcium fly ash, and the high-calcium fly ash based alkali activated binder as a function of time. The DTG peaks of the original high-calcium fly ash detected at 385, 605 and 965 °C indicate the decomposition of portlandite $Ca(OH)_2$, calcium carbonate $CaCO_3$ and anhydrite $CaSO_4$ respectively.

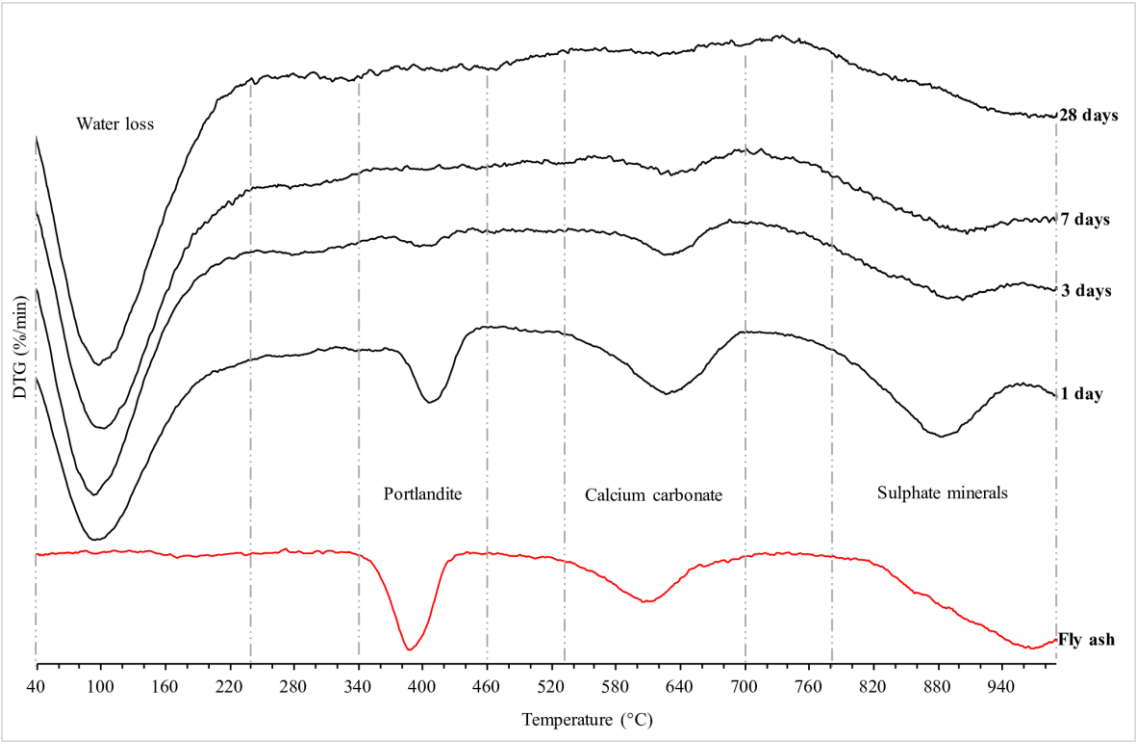

Fig. 2. DTG curves of raw fly ash and fly ash based alkali activated material F100 as a function of curing time.

The relatively low decomposition temperature of anhydrite compare to its theoretical decomposition at 1214°C [31] is ascribed to the fact that anhydrite is found interlinked with other calcium-rich phases by SEM (as illustrated later in section 3.1.4.1).

Regarding the alkali activated high-calcium fly ash, and complementary to XRD, thermogravimetric analyses confirm the consumption of portlandite $Ca(OH)_2$ over time. DTG curves also show the dissolution of calcium carbonate $CaCO_3$ with time. Finally, above 780 °C, the observed mass losses of the activated samples reveal the decomposition of sulphate minerals: anhydrite $CaSO_4$, thenardite Na_2SO_4 being formed from 3 days as detected earlier by XRD (see 3.1.1), for which theoretical polymorphic transformation occurs at around 900°C [32-33].

3.1.3 *Fourier Transform Infrared spectroscopy (FTIR)*

Fig. 3A shows FTIR spectra of the original high-calcium fly ash, and the high-calcium fly ash based alkali activated binder as a function of time in the range of CO_3^{2-} stretching vibrations.

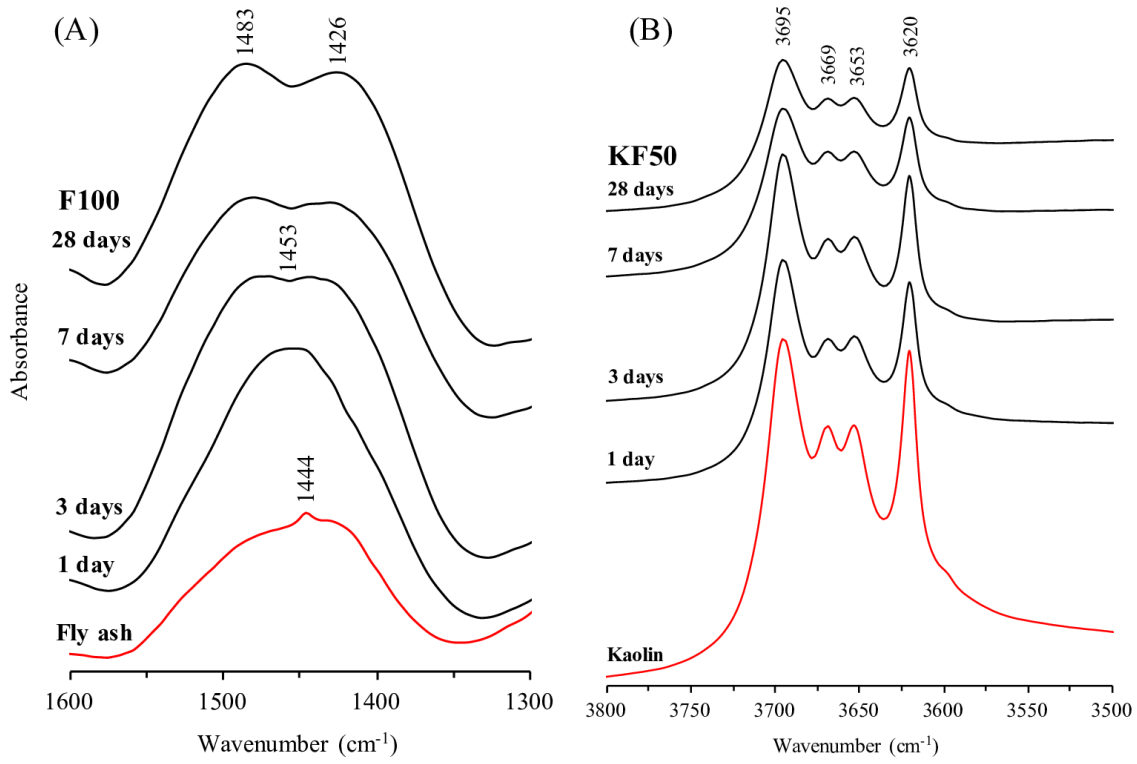

Fig. 3. FTIR of raw fly ash and fly ash based alkali activated material F100 as a function of curing time in the CO_3^{2-} stretching vibrations range (A) and raw kaolin and alkali activated kaolin KF50 as a function of curing time in the OH stretching vibrations range (B).

Different features of the CO_3^{2-} band is observed over time: at 1 day a single band around 1453 cm^{-1} is seen, while at 28 days a doublet positioned at 1426 and 1483 cm^{-1} is observed. Those modifications validate the formation of calcium carbonate during the curing time as observed by DTG.

Finally, Fig. A.1 (see appendices) shows FTIR spectra in the area of sulphate minerals. It confirms the dissolution of calcium sulphate (anhydrite, $CaSO_4$) along with the subsequent formation of sodium sulphate (thenardite, Na_2SO_4) as previously seen by XRD (see 3.1.1).

3.1.4 Scanning Electron Microscopy (SEM)

3.1.4.1 Calcium-rich phases

Fig. 4 shows SEM observations of the alkali activated high-calcium fly ash at 1 day. More specifically, it focuses on calcium-rich phases previously detected as reactive phases being dissolved following the alkali attack by XRD, TGA and FTIR.

Calcium-rich phases are initially present in high-calcium fly ash as nodules of large size from 100 to 250 μm. Besides, it is seen that chemical elements such as calcium, sulphur and silicon are not homogeneously spread within nodules suggesting a varying mineralogy. For instance, in area 2, despite a high content of sulphur indicating a prevalence of anhydrite ($CaSO_4$), the detected percentage of SO_3 with respect to CaO remains too low to be owed to the presence of anhydrite phases only. It is therefore concluded that the various calcium-containing phases such as anhydrite $CaSO_4$, calcite $CaCO_3$ and portlandite $Ca(OH)_2$ (previously detected by XRD and DTG in section 3.1.1 and 3.1.2) are interlaced within those nodule structures which represent reactive structures under alkaline attack.

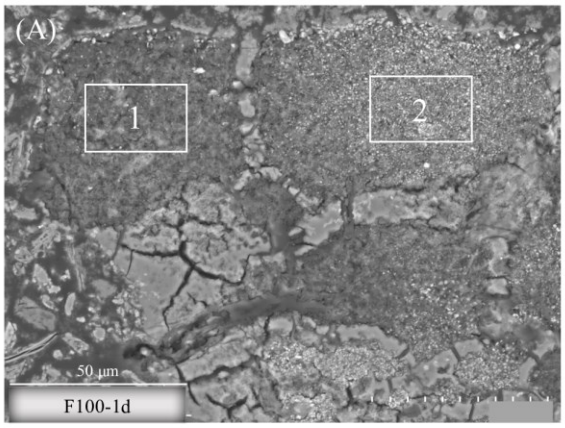

(B)

Wt. %	1	2
CaO	75.8	56.0
SO_3	11.5	39.7
SiO_2	12.7	4.3

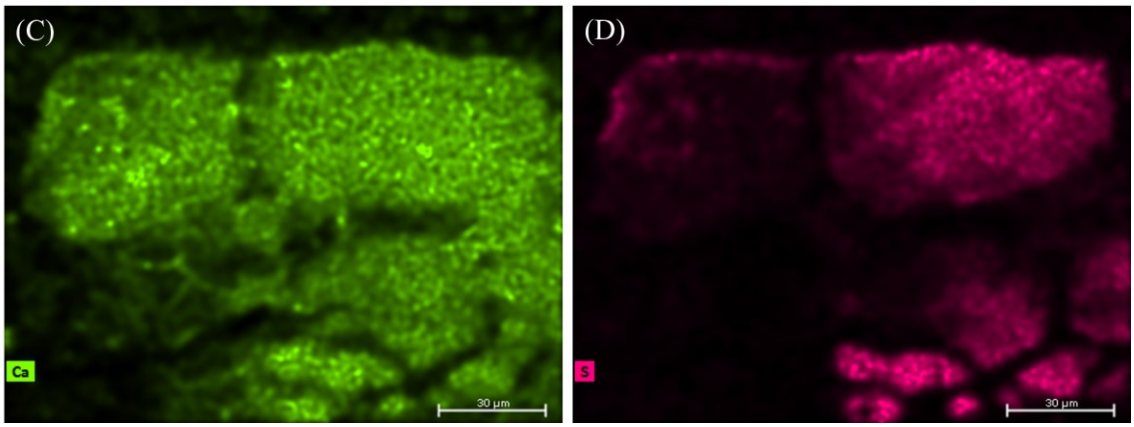

Fig. 4. SEM observations of a calcium-rich nodule from the alkali activated fly ash at 1 day: (A) SEM micrograph, (B) chemical composition (wt. %) of areas 1 and 2, (C) and (D) chemical mappings of calcium and sulphur respectively.

Overall sample

Fig. 5 additionally shows microstructural observations of the alkali activated high-calcium fly ash binder. At 1 day (Fig. 5A), a porous material along with distinct unreacted high-calcium fly ash particles is seen. In contrast, at 28 days (Fig. 5B), a more compact material with less pores is observed evidencing the formation of new compounds. Moreover, at 28 days, several unreacted high-calcium fly ash particles are still observed especially from the vitreous phase i.e. spherical and vesicular particles (see Fig. 5B, C and D).

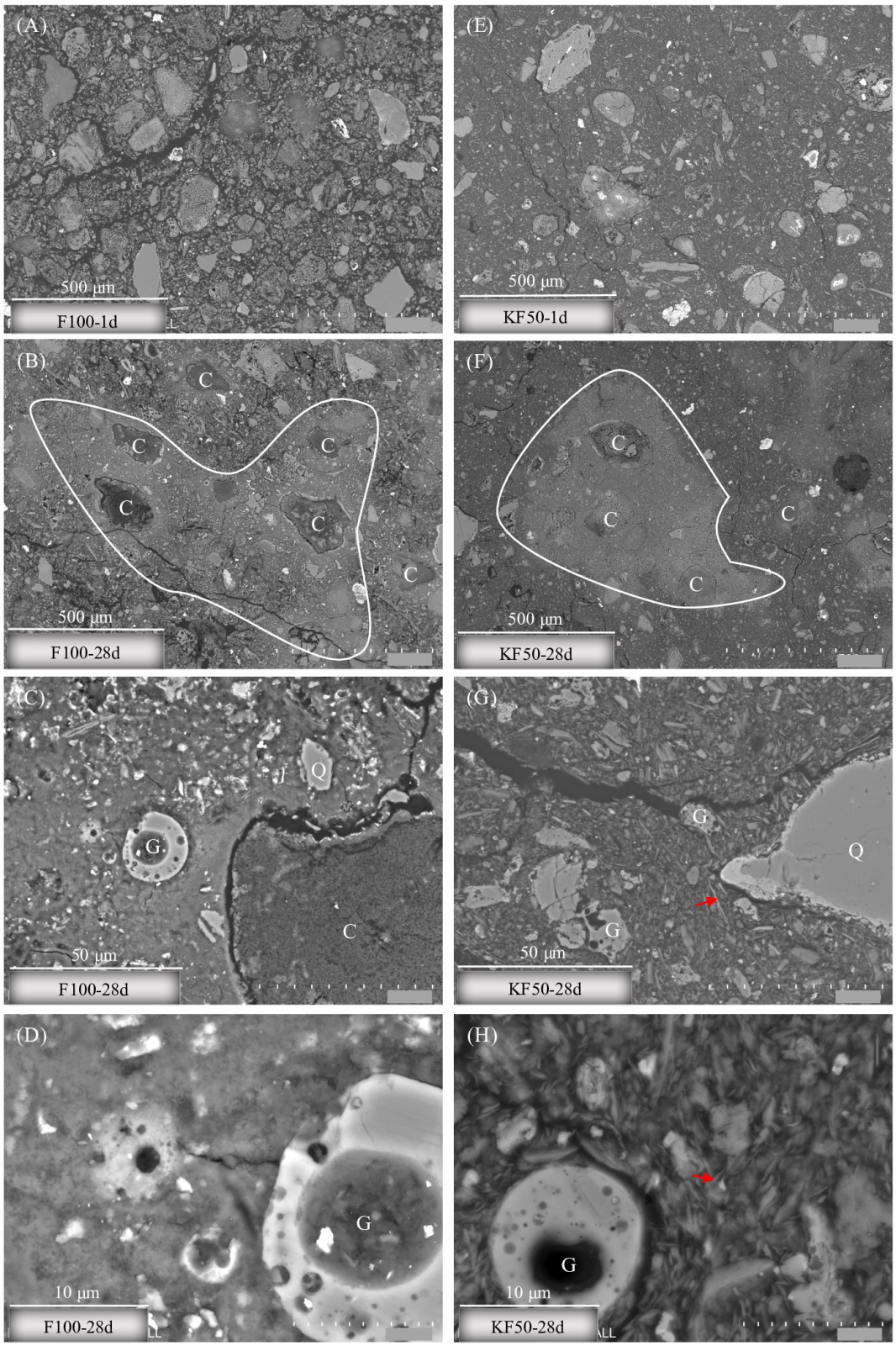

242

243 Fig. 5. SEM micrographs of (i) the alkali activated fly ash binder F100 (Column 1) (A) at 1 day and (B), (C) and (D)
244 at 28 days, (ii) the alkali activated kaolin KF50 (Column 2) (E) at 1 day and (F), (G) and (H) at 28 days; C=calcium
245 nodules; G=glass; Q=quartz.

Additional chemical analyses revealed that changes in microstructure are more significant around calcium-rich particles which were previously detected as the main reactive part of the raw high-calcium fly ash.

As a matter of fact, SEM micrographs show zones of higher density appearing brighter around calcium-rich nodules (see encircled area in Fig. 5B).

Table 3 gives an average chemical composition of the denser reactive areas. Notably, it indicates a ratio of sodium to sulphur around 2 matching with that of precipitated thenardite whose formula is Na_2SO_4, and implying that most of the sodium from the alkaline solution is taken up to form thenardite.

Table 3

Average elemental composition (wt. %) of F100 and KF50 denser areas at 28 days.

	Si	Ca	Al	Na	S	K	Fe	Mg	O
F100-28d	22.1	19.2	7.0	3.7	1.7	1.2	0.8	0.5	43.8
KF50-28d	24.1	14.5	8.8	3.1	1.6	1.6	0.7	0.3	45.3

Furthermore, Table 3 indicates that the massive reactive area is primarily composed of silicon and calcium. Supposing that the new compounds are mainly located in those denser areas, these results suggest that apart from thernardite the new compounds are enriched in silicon and calcium.

3.1.5 Nuclear Magnetic Resonance (NMR)

Nuclear Magnetic Resonance was finally used to follow amorphous phases and precise the structure of the new compounds formed in our investigated system.

Fig. 6 shows ^{27}Al MAS-NMR spectrum of the original high-calcium fly ash as well as the spectrum belonging to the alkali activated high-calcium fly ash at 28 days. ^{27}Al NMR spectrum of the original high-calcium fly ash displays two resonances whose

dissymmetrical shapes are due to electric field gradient distribution caused by the distribution of geometries of the AlO4 and AlO6 polyhedra.. More specifically, the main resonance whose maximum is detected at 55 ppm corresponds to Al(IV) of the vitreous phase. While the resonance located at 3 ppm corresponds to Al(VI) of the vitreous phase.

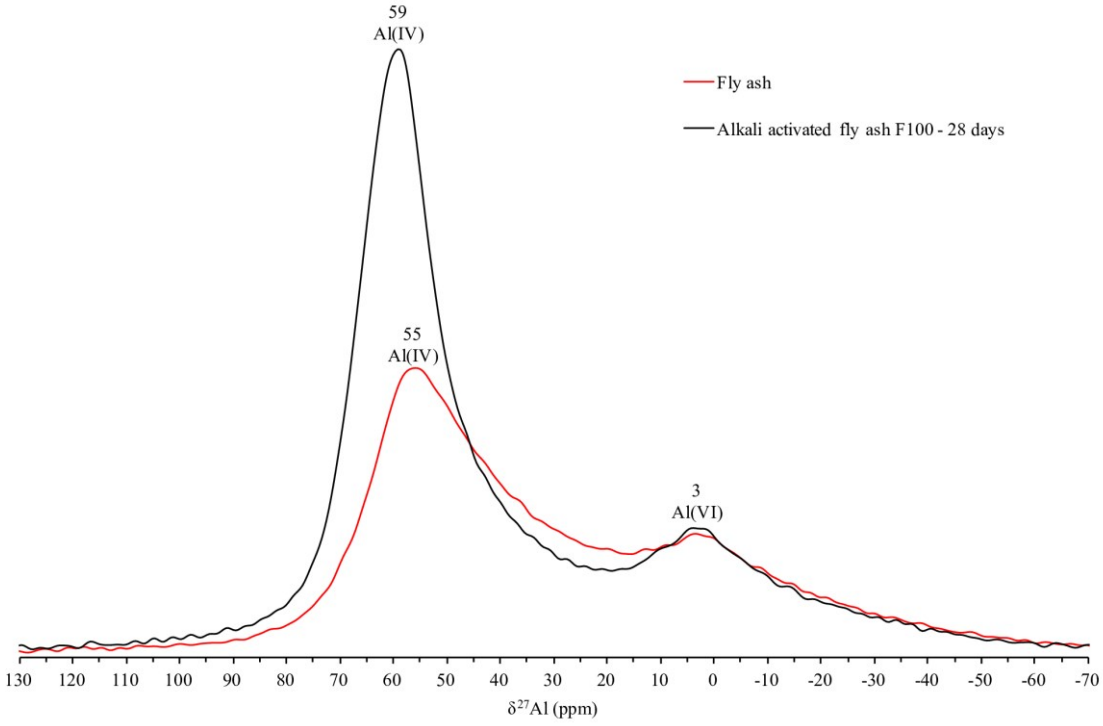

Fig. 6. ^{27}Al MAS-NMR spectra of the raw fly ash and alkali activated fly ash at 28 days.

Comparatively, the high-calcium fly ash based alkali activated material spectrum at 28 days exhibits a main resonance sharper and a maximum shifted to 59 ppm corresponding to four-fold coordination of aluminium namely $q^4(4Si)$. Those modifications in the spectrum compared to the original high-calcium fly ash indicate that part of the aluminium released from high-calcium fly ash leads to the formation a new aluminium bearing phase whose aluminium is tetrahedrally coordinated. Lastly, the resonance owed to octahedral aluminium at 3 ppm is still present which means that high-calcium fly ash is not totally dissolved after 28 days.

283 Fig. 7 shows ^{29}Si MAS-NMR spectra of the original high-calcium fly ash as well as the
284 alkali activated high-calcium fly ash at 28 days. ^{29}Si NMR spectrum of the original high-
285 calcium fly ash shows a broad resonance between -85 and -105 ppm attributed to the
286 presence of a wide range of Q^3 and Q^4 silicon local environments from the vitreous phase.

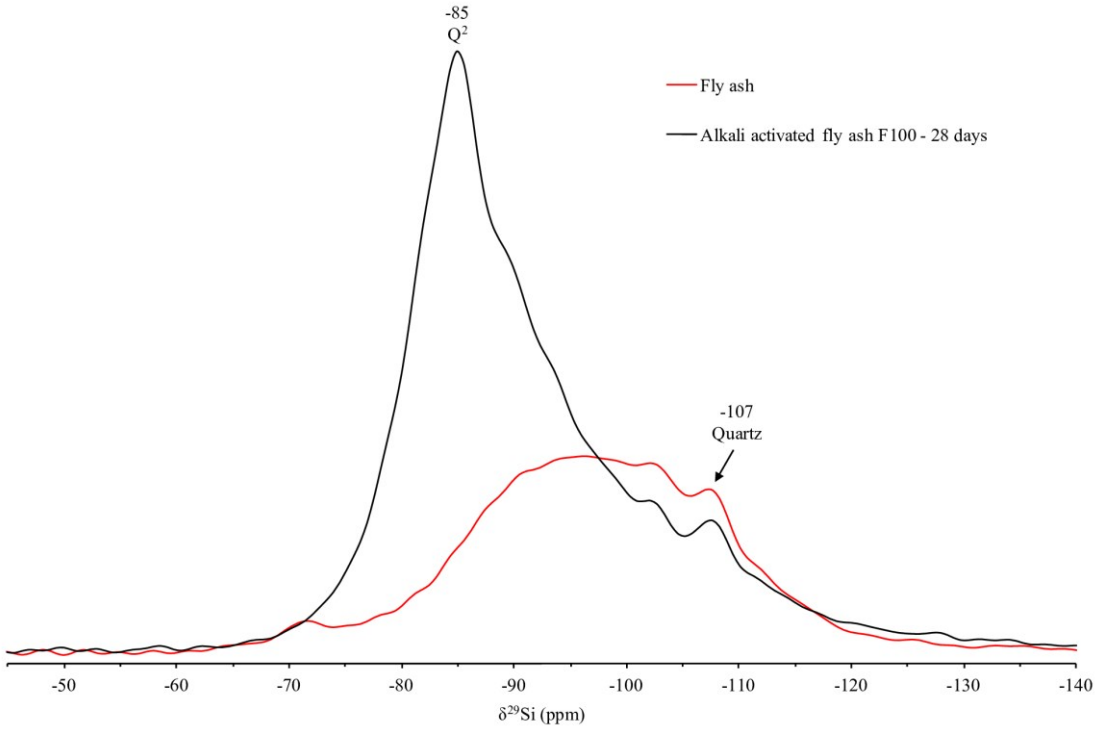

287

288 Fig. 7. ^{29}Si MAS-NMR spectra of the raw fly ash and alkali activated fly ash at 28 days.

289 In contrast, the alkali activated high-calcium fly ash spectrum at 28 days displays a clear
290 additional resonance centred at -85 ppm. This new position can be attributed to both the
291 formation of Q^4(4Al) or else Q^2-type silicon environments. Nevertheless, regarding the
292 high value of the Si/Al ratio around 3.2 in the denser area comprising the new products,
293 and measured by SEM (see Table 3) it is unlikely that Q^4(4Al) environments are present.
294 The new resonance at -85 ppm consequently indicates the formation of Q^2-type silicon
295 environments in chain structure. Considering that the spectrum does not show any
296 resonance corresponding to Q^1 silicon environments the length of those formed chains is
297 high. It is also worth noting that Q^2 Si environments in chain possess a charge deficit of

298 2- which must be compensated. However, sodium cations are not available as they are
299 associated with sulphur to form thenardite Na_2SO_4 (see sections 3.1.1 and 3.1.3).
300 Consequently, only calcium cations released from calcium reactive phases of high-
301 calcium fly ash can compensate this charge deficit. Those silicon chain structures are
302 therefore combined with dissolved calcium which matches with the chemical
303 composition of the denser reactive area primarily made of silicon and calcium (see Table
304 2). The significant broadening of the resonance at -85 ppm also indicates that those chains
305 are not well organised as C–S–H structures generally observed in Portland cement [34].
306 Considering the low Ca content of the raw fly ash, the line broadening fully agrees with
307 amorphous C-S-H with a low Ca/Si ratio.
308 Finally, the broadest part of the activated high-calcium fly ash spectrum at 28 days from
309 -90 ppm to -100 pm indicates the presence of Q^3 and Q^4 environments mainly issued from
310 the remaining vitreous phase of high-calcium fly ash, and in accordance with the previous
311 observations of unreacted high-calcium fly ash particles at 28 days by SEM (see 3.1.4.2).
312 In summary, both ^{29}Si and ^{27}Al MAS-NMR spectroscopy indicates the formation of new
313 signals following alkaline activation. It is of interest to understand whether the new
314 aluminium-containing phase seen in ^{27}Al NMR correlates with the silicate chain structure
315 observed in ^{29}Si NMR. As a comparison, aluminium in linear structure such as C–S–H is
316 either found (i) as Q^2 environments corresponding to aluminium substituting for silicon
317 atoms, and located around 68-74 ppm in ^{27}Al NMR or else (ii) as Q^3 environments
318 corresponding to crosslinking through alumina bridging tetrahedra positioned around 63-
319 68 ppm in ^{27}Al NMR [35-37]. However, as mentioned above, the new aluminium
320 resonance observed in our investigation at 59 ppm would rather correspond to $q^4(4Si)$
321 environment. Consequently, if aluminium is incorporated into the silicate chain structure,

322 it would be in a three-dimensional environment which has not been described in literature
323 yet.To conclude, results concerning the alkali activated high-calcium fly ash binder
324 showed that calcium-rich phases constitute the reactive part of the raw high-calcium fly
325 ash, while its vitreous phase remains mainly unreactive. The new compounds formed are
326 mainly located around calcium-rich reactive particles and present a complex chemistry
327 and structure which differ from cementitious compounds generally encountered in
328 cement or lime based system.
329
330 *3.2 Interaction between the alkali activated high-calcium fly ash binder and kaolin*
331 The following section aims at understanding the interaction between kaolin and the alkali
332 activated high-calcium fly ash binder previously described. More specifically, it aims at
333 answering the following question: does the presence of kaolin modify the reaction
334 sequence?
335 Two stabilised soils were studied i.e. KF50 for which the solid phase is made in mass of
336 50% of high-calcium fly ash and 50% of kaolin, and KF20 made of 20% of high-calcium
337 fly ash and 80% of kaolin. Observations made for these two mixes turned out to be similar
338 for all the techniques used. Therefore, only the results of KF50 will be shown while the
339 results of KF20 can be found in Supporting Information.
340
341 Firstly, Fig. 3B shows the infrared spectrum of the original kaolin as well as the spectra
342 belonging to the alkali activated soil KF50 as a function of time. The four bands observed
343 in the 3695–3620 cm^{-1} range are typical of the presence of kaolinite, and arise from the
344 vibration of its internal OH groups. Notably, disorder in kaolinite is mainly detectable in
345 this OH-stretching region by FTIR [38]. Those bands being still observed over time in

346 the alkali activated soils suggest that kaolinite does not react under alkaline conditions.
347 The smaller heights seen at 7 and 28 days are only due to higher sample densities at higher
348 curing times after the formation of new compounds, leading to smaller probed distance
349 and therefore lesser absorbance.
350
351 Fig. A.3 (see appendices) shows XRD patterns of the activated soil KF50 as a function
352 of curing time. Similarly to the alkali activated high-calcium fly ash binder (see 3.1.1), it
353 indicates the dissolution of anhydrite $CaSO_4$ along with the formation of thenardite
354 Na_2SO_4.
355
356 Fig. 5E, F, G and H shows microstructural observations of the alkali activated kaolin
357 KF50. At 1 day, and in contrast with the alkali activated high-calcium fly ash (Fig. 5A),
358 KF50 presents a relatively low porosity due to the presence of small-sized kaolinite
359 platelets filling the pores (Fig. 5E). At 28 days, and in a similar way to the activated high-
360 calcium fly ash (Fig. 5B), KF50 presents a more compact microstructure around calcium-
361 rich phases (see encircled area in Fig. 5F).
362 Furthermore, by comparing the alkali activated high-calcium fly ash binder (Fig. 5C and
363 D) with the activated soil KF50 (Fig. 5G and H), kaolinite platelets are distinctly observed
364 (see red arrows as an example of platelet observation), and homogeneously spread across
365 the whole sample. In fact, kaolinite platelets were observed not merely in the matrix but
366 also in the most reactive massive areas supporting that kaolinite does not react even in
367 the reactive areas but rather acts as a filler.
368 Table 2 gives an average chemical composition of KF50 massive areas. It shows similar
369 tendencies than for the alkali activated high-calcium fly ash binder F100. Only slightly

higher contents of silicon and aluminium are measured for KF50 due to the presence of kaolinite.

Fig. 8 shows ^{27}Al MAS-NMR spectra of the alkali activated high-calcium fly ash binder F100 studied in the first section, and the alkali activated soil KF50 at 1 and 28 days. By comparison with the binder F100, ^{27}Al NMR spectroscopy of KF50 displays two additional resonances due to the presence of kaolin i.e. a main resonance at 4 ppm due to Al(VI) of the octahedral layer of kaolinite, and a resonance at 70 ppm owed to Al(IV) and corresponding to substitution of Al for Si in the tetrahedral layer of kaolinite and muscovite.

At 1 day, KF50 presents a resonance whose maximum is located at 55 ppm and owed to the vitreous phase of high-calcium fly ash, while at 28 days a shift of this resonance to 58 ppm indicates the formation of tetrahedral aluminium in q^4(4Si) environments (as previously described for the alkali activated high-calcium fly ash in section 3.1.5).

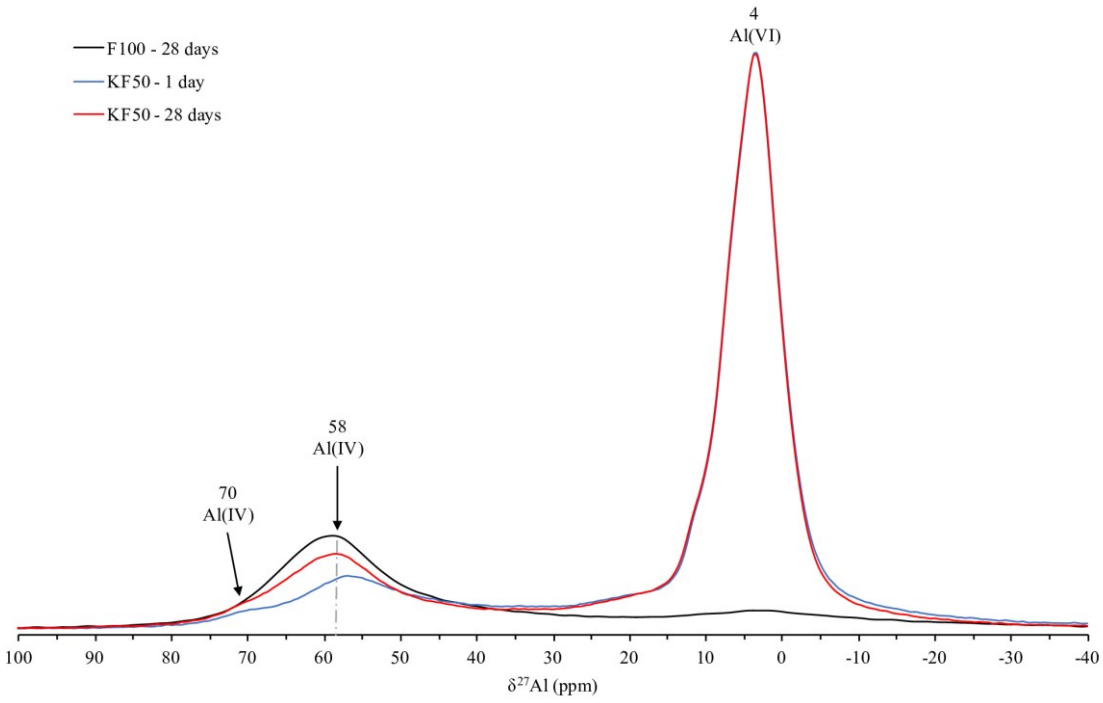

Fig. 8. ^{27}Al MAS-NMR spectra of the alkali activated fly ash F100 at 28 days and alkali activated kaolin KF50 at 1 and 28 days.

Fig. 9 shows ^{29}Si MAS-NMR spectra of the alkali activated high-calcium fly ash binder F100 studied in the first section, and the alkali activated soil KF50 at 1 and 28 days. ^{29}Si NMR spectroscopy of KF50 samples show an additional thin resonance at -91 ppm corresponding to the silicon of the tetrahedral layer of kaolinite. This resonance does not undergo any modification over time confirming the non-reactivity of kaolinite.

Furthermore, from 1 to 28 days KF50 shows the clear appearance of a resonance at -85 ppm due to the formation of silicon chains combined with dissolved calcium, and as previously described for the alkali activated high-calcium fly ash binder (see 3.1.5).

To conclude, results of this second section showed that kaolin is unreactive during alkaline attack. Besides, a similar reaction sequence than for the alkali activated high-calcium fly ash binder occurs.

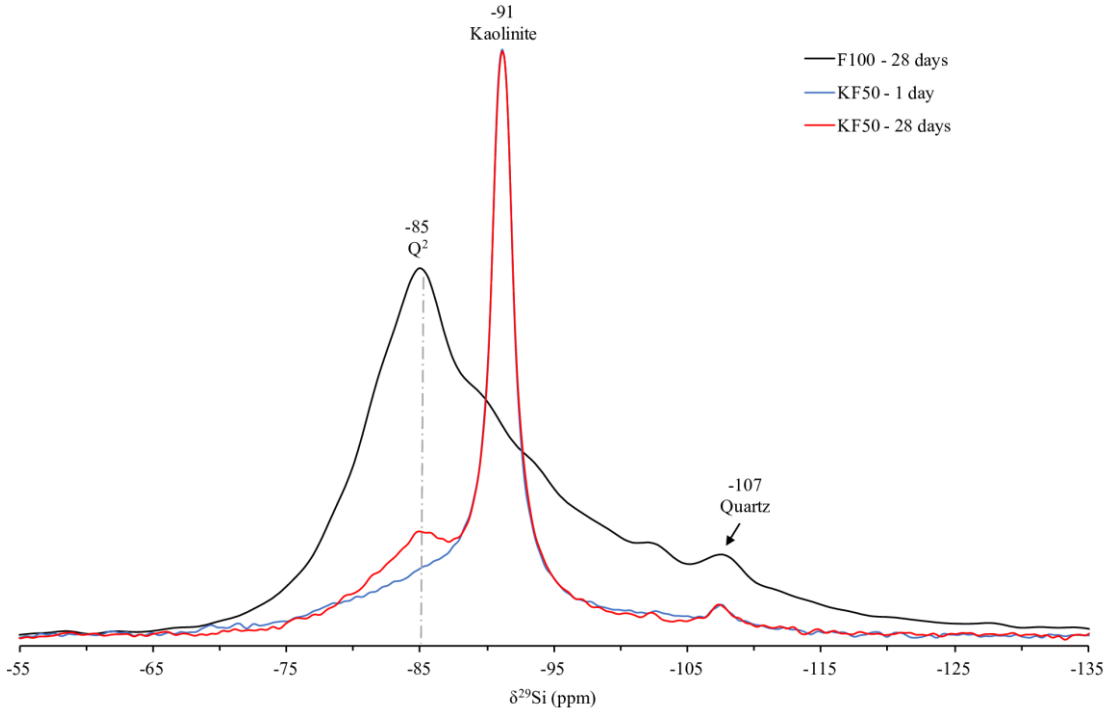

Fig. 9. ^{29}Si MAS-NMR spectra of the alkali activated fly ash F100 at 28 days and alkali activated kaolin KF50 at 1 and 28 days.

3.3 Comparison with lime treated kaolin

This last section focuses on a comparison with previous studies which reported the physicochemical evolution of the same kaolin treated either by a common stabiliser: lime [6], but also treated by a mix of lime and the high-calcium fly ash used here [39].

Table 4 gives a summary of the reaction sequences for each system highlighting strong differences. This section consequently aims at providing a better understanding of the consequences of those variable reaction sequences on the final material in terms of performance and durability.

Table 4

Compared reactivity sequences of kaolin treated either by lime, or a mix of lime and fly ash or an alkali activated fly ash

		Kaolin + Lime [6]	Kaolin + Lime + Fly ash [33]	Kaolin + Alkali activated fly ash
1. Phases dissolved		Kaolin, lime	Kaolin, lime, fly ash	Fly ash
2. Reactivity timescale		Slow	Fast	Fast
3. Phases formed	Aluminate	Calcium Aluminate Hydrate C–A–H Monocarboaluminate hydrate C_4–A–C–H_{11}	Calcium Aluminate Hydrate C–A–H Calcium Aluminium Oxide Carbonate Hydrate C–A–O–C–H Calcium Aluminium Oxide Hydrate C–A–O–H Ettringite $Ca_6Al_2(SO_4)_3(OH)_{12}.26H_2O$	Amorphous silicate consisting of chains combined with calcium - and probably incorporating the observed q4(4Si) aluminium environments
	Silicate	None	Calcium Silicate Hydrate C–S–H	

3.3.1 Reactivity of initial phases

Firstly and regarding the reactivity of the phases initially present, it was found that kaolin is inert in our alkali activated samples which contrasts with the two other lime based systems for which kaolinite is dissolved. The limited reactivity of kaolinite in the alkali activated soils herein studied is due to the presence of other more reactive phases. Besides, its limited reactivity is beneficial for the system as no side effects will occur.

For the three systems, calcium-containing phases constitute the main reactive part of the mixes playing a pivotal role in the reaction development scheme. In fact, their dissolution leads to the release of dissolved calcium into the medium and hence pozzolanic activity i.e. formation of new calcium cementitious compounds responsible of the strength improvement. In the case of our alkali activated soils however, it is not lime CaO that constitutes a supply of calcium but calcium-containing minerals from high-calcium fly ash $CaSO_4$, $CaCO_3$ or $Ca(OH)_2$. For all calcium-source types the supply of Ca^{2+} cations remains identical. What changes is the anion simultaneously released from their dissolution: when high-calcium fly ash is present the dissolution of its calcium-containing minerals is accompanied by the release of various anions such as OH^-, SO_4^{2-} and CO_3^{2-}

430 influencing the reaction sequence, and with potential negative effects for the durability
431 as seen later.
432 Finally, concerning the vitreous phase of high-calcium fly ash, although amorphous and
433 hence metastable it showed few reactivity leading to a preferential pozzolanic activity as
434 seen in Portland cement, rather than polymerisation reactions associated with the
435 formation of an aluminosilicate three-dimensional network characteristic of low-calcium
436 alkali activated materials and geopolymers.
437 *3.3.2 Reactivity timescale*
438 Reactions in presence of high-calcium fly ash are fast with new compounds already
439 observed at 28 days for both systems made of kaolin, lime and high-calcium fly ash [39]
440 but also kaolin and alkali activated high-calcium fly ash. Whereas, longer reactivity
441 timescale occurs for lime treated kaolin: new cementitious compounds being previewed
442 from 60 days and clearly detected only after 270 days [6].
443 For a system made of lime and kaolin its pozzolanic activity depends on the dissolution
444 of kaolinite which constitutes the only source of aluminium and silicon. Considering that
445 kaolinite possesses a stable crystalline mineral structure hard to dissolve it explains the
446 slow reactivity of that system. By contrast, high-calcium fly ash contains reactive phases
447 i.e. calcium-rich phases primarily and to a small extent its vitreous phase (for the high-
448 calcium fly ash used here) thermodynamically less stable than kaolinite and therefore
449 easier to dissolve. That is why reaction sequences are faster for both high-calcium fly ash
450 systems. It is even faster for our alkali activated soils as the alkaline solution brings a
451 mixture of ions ready available. Those fastest reaction times would constitute an
452 advantage in the case where the quickly formed products are as well stable binding phases
453 which will be discussed now.

3.3.3 Stability and structure of the compounds formed

In the case of formerly studied systems made of kaolin and lime as well as kaolin, lime and high-calcium fly ash, a preferential release of aluminium over silicon from kaolinite and/or high-calcium fly ash dissolution occurs conducting to the formation of aluminium compounds primarily. In fact, for a lime treated kaolin Calcium Aluminate Hydrate C–A–H and monocarboaluminate hydrate C_4–A–C–H_{11} are formed [6]. In the case of a kaolin treated by a mix of lime and high-calcium fly ash Calcium Aluminate Hydrate C–A–H but also Calcium Aluminium Oxide Carbonate Hydrate C–A–O–C–H, Calcium Aluminium Oxide Hydrate C–A–O–H and Ettringite $Ca_6Al_2(SO_4)_3(OH)_{12}.26H_2O$ are formed [39]. Whereas, in our alkali activated soils investigated here, aluminium dissolved from the vitreous phase of high-calcium fly ash was found in a three-dimensional four-fold environment (q^4(4Si)) which strongly contrasts with the six-fold environments found in the Calcium Aluminate Hydrates.

Regarding the formation of silicate compounds, none are formed in a system made of kaolin and lime [6] because the dissolution of kaolinite is slow and starts by the release of its aluminium. Hence, no silicon is made available. Kaolinite being the only source of silicon in that system the limited dissolution of silicon implies the non-formation of silicon compounds. By contrast in a kaolin, lime and high-calcium fly ash system, the dissolution of silicon from the vitreous phase of high-calcium fly ash leads to the formation of Calcium Silicate Hydrate C–S–H [39]. Finally, in the alkali activated soils herein studied, the supply of silicon from the alkaline solution primarily and also from the vitreous phase of high-calcium fly ash leads to the formation of silicon chains combined with calcium, but whose NMR signature greatly differs from C–S–H commonly observed as described above (see section 3.1.5). It is also likely that aluminium

478 found in three-dimensional four-fold environment (q^4(4Si)) is incorporated into those
479 silicon chains.
480 Calcium Silicate Hydrate C–S–H is the principal binding phase of Portland cement and
481 concrete primarily responsible for its strength [40]. In addition, its structure is more stable
482 than Calcium Aluminate Hydrates [41]. Their presence is consequently beneficial for the
483 performances. The fact that in our alkali activated samples, a diverse structure compared
484 to usual C–S–H is observed cannot easily be assessed in term of stability at the present
485 moment. Indeed, regarding the lack of crystallinity of our silicon chains formed,
486 experience proved that the crystallinity of the binding agent alone constitutes a poor
487 measure of stability over the timescales relevant to the majority of concrete structures
488 [41]. A further investigation of the performances would help apprehending a potential
489 beneficial effect of this uncommon silicon chains structure over time.
490
491 Finally, for both high-calcium fly ash systems, sulphate minerals are formed: either
492 Ettringite $Ca_6Al_2(SO_4)_3(OH)_{12}.26H_2O$ for a system made of kaolin, lime and high-
493 calcium fly ash [39], or Thenardite Na_2SO_4 in our alkali activated soils.
494 Their formation is due to the dissolution of anhydrite $CaSO_4$ initially present in the high-
495 calcium fly ash, and releasing sulphate anions SO_4^{2-} that are subsequently recombining
496 with available cations. For the case of a kaolin, lime and high-calcium fly ash system the
497 formation of Ettringite is taking up aluminium and calcium hence slowing down both the
498 simultaneous formation of aluminate and silicate hydrates. Whereas, in our alkali
499 activated system, sodium cations ready available from the alkaline solution combine with
500 sulphate anions. Therefore, the formation of sulphate minerals does not affect the parallel
501 development of the pozzolanic activity i.e. the formation of silicate chains. Finally, a key

point to consider for durability aspects is the high solubility of sulphate minerals which are few stable salts in water. In fact, a previous study in which leaching tests were performed on an alkali activated sulphate-bearing kaolin showed that the uptake of sulphate anions by the gel is low, namely less than 40% [42]. The study of the effect of wetting-drying cycles is consequently warranted to verify a further impact of the presence of thenardite on the long-term performances.

3 Conclusions

Here, the development of a novel soil binder that is an alkali activated calcium-rich high-calcium fly ash for clay soil stabilisation was explored. The study of its reactivity showed that (i) the overall calcium-bearing minerals from high-calcium fly ash constitute the reactive phases while its vitreous phase remains mainly unreactive, (ii) new compounds are formed, thenardite Na_2SO_4 and an amorphous silicate consisting of chains combined with calcium - (iii) reactions happen within 1 to 28 days.

The interaction between the binder developed and the model soil chosen i.e. kaolin, showed that kaolin is unreactive. Its presence whatever the proportion does not modify the physicochemical evolution of the system that is neither the dissolved phases, formed compounds, nor reactivity timescale. The inert kaolinite platelets were in addition found homogenously embedded in the matrix acting as a filler.

When compared to lime treated kaolin, although pozzolanic activity remains the dominant process reaction sequences are strongly different. In the case of alkali activated soils the formation of calcium-silicon chains phases more stable than calcium aluminium hydrates encountered in lime based systems is beneficial for long-term stability purpose. Those observed silicon chains however show an uncommon structure whose effect on the performances will be checked in a future investigation. Finally, the formation of

thenardite a highly soluble salt in water raises interest about the durability of the material which will be also further investigated.

Acknowledgements

The authors wish to acknowledge the support of the European Commission via the Marie Skłodowska-Curie Innovative Training Networks (ITN-ETN) project TERRE 'Training Engineers and Researchers to Rethink geotechnical Engineering for a low carbon future' (H2020-MSCA-ITN-2015-675762).

Appendices

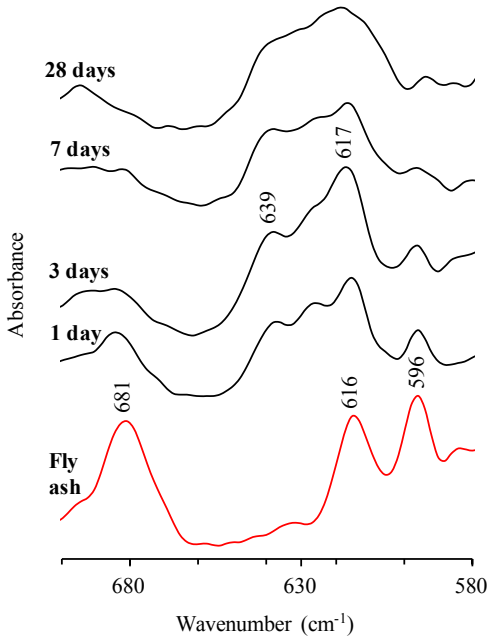

Fig. A.1. FTIR of raw high-calcium fly ash, and high-calcium fly ash based alkali activated material F100 as a function of curing time in the SO_4^{2-} stretching vibrations range; 681, 616 and 596 cm^{-1} = anhydrite CaSO4; 639 and 617 cm^{-1} = thenardite Na_2SO_4.

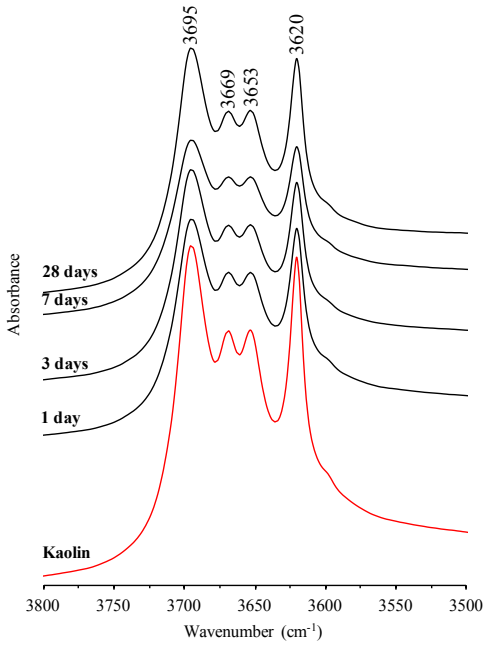

Fig. A.2. FTIR of the raw kaolin and alkali activated kaolin KF20 as a function of curing time in the OH stretching vibrations range.

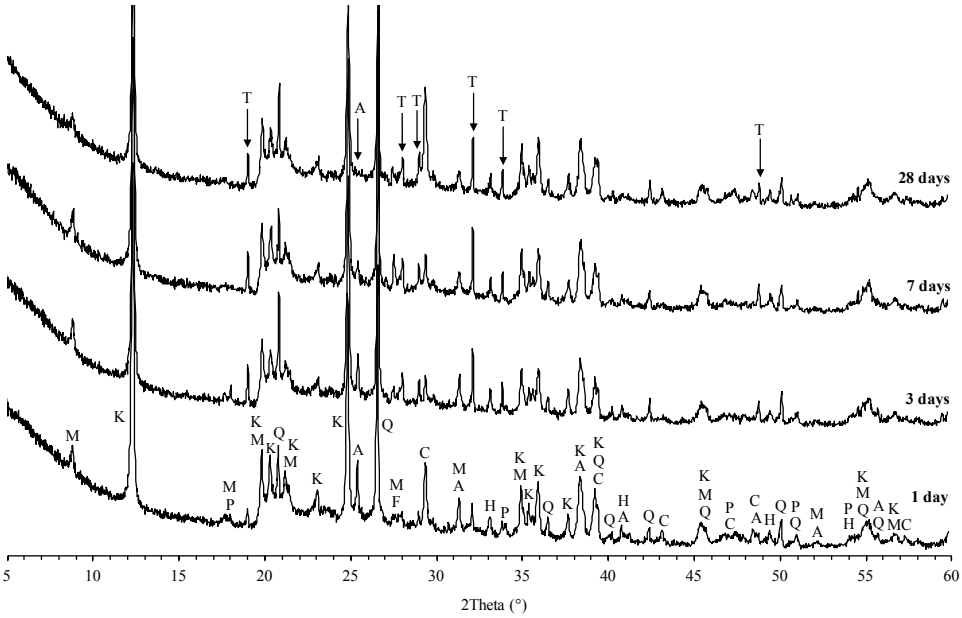

Fig. A.3. XRD of alkali activated kaolin KF50 as a function of curing time; A=anhydrite; C=calcite; F=feldspar; H=hematite; K=kaolinite; M=muscovite; P=portlandite; Q=quartz; T=thenardite.

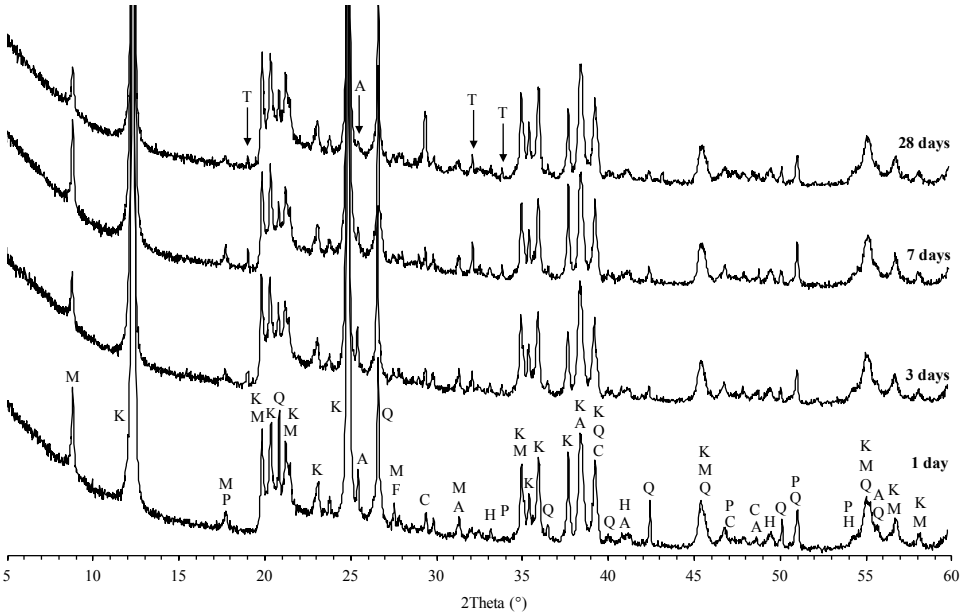

548

549 Fig. A.4. XRD of the alkali activated kaolin KF20 as a function of curing time;

550 A=anhydrite; C=calcite; F=feldspar; H=hematite; K=kaolinite; M=muscovite;

551 P=portlandite; Q=quartz; T=thenardite.

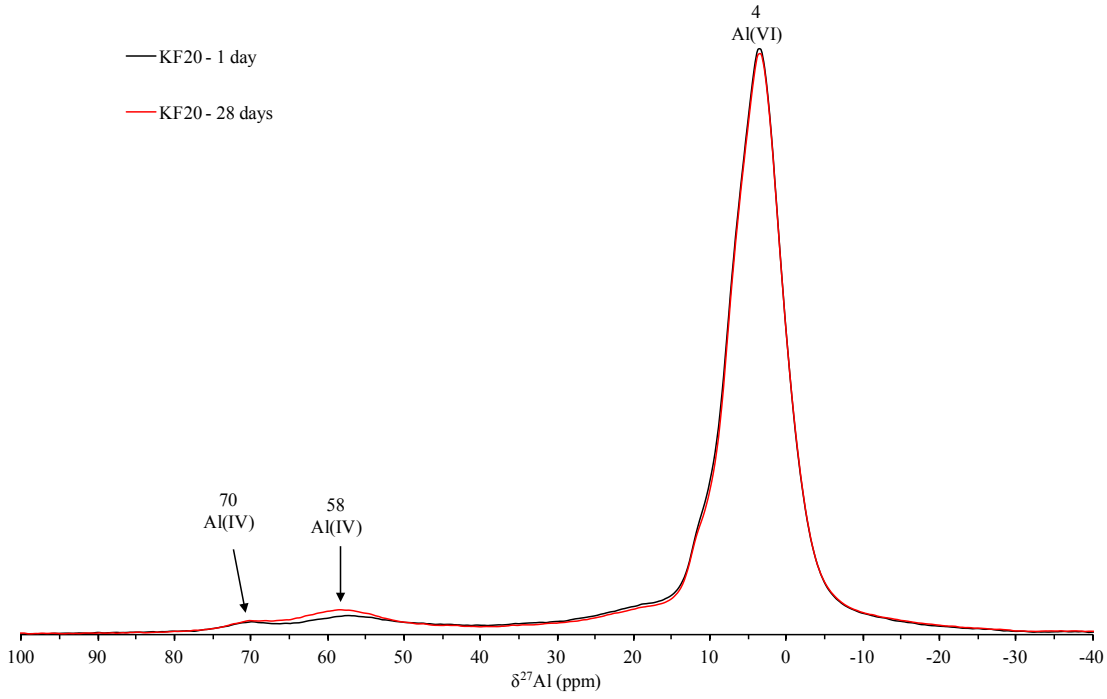

552

553 Fig. A.5. ^{27}Al MAS-NMR of the raw high-calcium fly ash, raw kaolin and alkali

554 activated kaolin KF20 at 0 and 28 days.

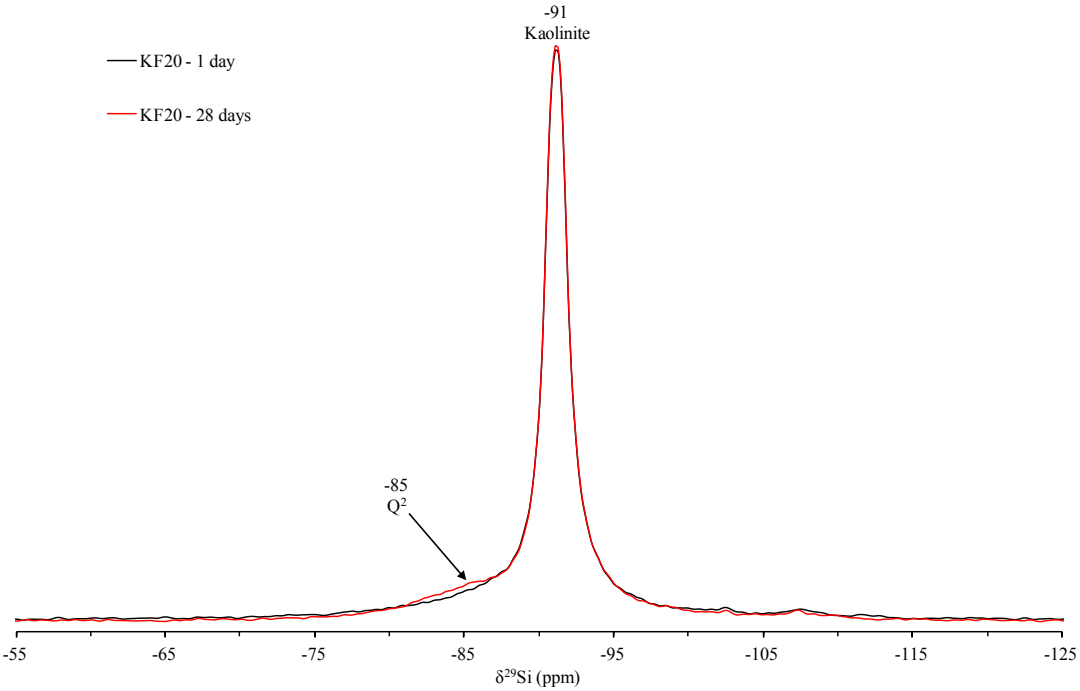

Fig. A.6. ^{29}Si MAS-NMR of the raw high-calcium fly ash, raw kaolin and alkali activated kaolin KF20 at 0 and 28 days.

References

[1] Pomakhina, E., Deneele, D., Gaillot, A.-C., Paris, M., Ouvrard, G., 2012. ^{29}Si solid state NMR investigation of pozzolanic reaction occurring in lime-treated Ca-bentonite. Cem. Concr. Res. 42, 626–632.

[2] Lemaire, K., Deneele, D., Bonnet, S., Legret, M., 2013. Effects of lime and cement treatment on the physicochemical, microstructural and mechanical characteristics of a plastic silt. Eng. Geol. 166, 255–261.

[3] Chemeda, Y.C., Deneele, D., Christidis, G.E., Ouvrard, G., 2015. Influence of hydrated lime on the surface properties and interaction of kaolinite particles. Appl. Clay Sci. 107, 1–13.

[4] Deneele, D., Le Runigo, B., Cui, Y. J., Cuisinier, O., Ferber, V., 2016. Experimental assessment regarding leaching of lime-treated silt. Constr. Build. Mater. 112, 1032– 1040.

[5] Maubec, N., Deneele, D., Ouvrard, G., 2017. Influence of the clay type on the strength evolution of lime treated material. Appl. Clay Sci. 137, 107–114.

[6] Vitale, E., Deneele, D., Paris, M., Russo, G., 2017. Multi-scale analysis and time evolution of pozzolanic activity of lime treated clays. Appl. Clay Sci. 141, 36–45.

[7] Guidobaldi, G., Cambi, C., Cecconi, M., Deneele, D., Paris, M., Russo, G., Vitale, E., 2017. Multi-scale analysis of the mechanical improvement induced by lime addition on a pyroclastic soil. Eng. Geol. 221, 193–201.

[8] Scrivener, K.L., Kirkpatrick, R.J., 2008. Innovation in use and research on cementitious material. Cem. Concr. Res. 38, 128–136.

[9] Rahman, A, 1986. The Potentials of Some Stabilizers for the Use of Lateritic Soil in Construction. Build. Environ. 21, 57–61.

[10] Basha, E.A., Hashim, R., Muntohar, A., 2003. Effect of the cement-rice husk ash on the plasticity and compaction of soil. Electron. J. Geotech. Eng. 8.

[11] Nalbantoğlu, Z., 2004. Effectiveness of Class C fly ash as an expansive soil stabilizer. Constr. Build. Mater. 18, 377–381.

[12] Kolias, S., Kasselouri-Rigopoulou, V., Karahalios, A., 2005. Stabilisation of clayey soils with high calcium fly ash and cement. Cem. Concr. Compos. 27, 301–313.

[13] Parsons, R.L., Kneebone, E., 2005. Field performance of fly ash stabilised subgrades. Ground Improv. 9, 33–38.

[14] Sharmaa, U., Khatrib, A., Kanoungoc, A., 2014. Use of Micro-silica as Additive to Concrete-state of Art. Int. J. Civ. Eng. Res. 5, 9–12.

[15] James, J., Pandian, P.K., 2016. Industrial Wastes as Auxiliary Additives to Cement/Lime Stabilization of Soils. Adv. Civ. Eng. 2016, 1–17.

[16] Singhi, B., Laskar, A.I., Ahmed, M.A., 2016. Investigation on Soil–Geopolymer with Slag, Fly Ash and Their Blending. Arab. J. Sci. Eng. 41, 393–400.

[17] Wilkinson, A., Haque, A., Kodikara, J., 2010. Stabilisation of clayey soils with industrial by-products: part A. Proc. Inst. Civ. Eng. - Ground Improv. 163, 149–163.

[18] Cristelo, N., Glendinning, S., Teixeira Pinto, A., 2011. Deep soft soil improvement by alkaline activation. Proc. Inst. Civ. Eng. - Ground Improv. 164, 73–82.

[19] Phummiphan, I., Horpibulsuk, S, Rachan, R., Arulrajah, A., Shen, S-L., Chindaprasirt, P. 2018. High Calcium Fly Ash Geopolymer Stabilized Lateritic Soil and Granulated Blast Furnace Slag Blends as a Pavement Base Material, Journal of Hazardous Materials, Journal of Hazardous Materials, 341, pp. 257-267

20] Cristelo, N., Glendinning, S., Fernandes, L., Pinto, A.T., 2012. Effect of calcium content on soil stabilisation with alkaline activation. Constr. Build. Mater. 29, 167–174.

626 [21] Rios, S., Cristelo, N., Viana da Fonseca, A., Ferreira, C., 2016. Structural
627 Performance of Alkali-Activated Soil Ash versus Soil Cement. J. Mater. Civ. Eng. 28,
628 4015125.
629
630 [22] Tenn, N., Allou, F., Petit, C., Absi, J., Rossignol, S., 2015. Formulation of new
631 materials based on geopolymer binders and different road aggregates. Ceram. Int. 41,
632 5812–5820.
633
634 [23] Sargent, P., Hughes, P.N., Rouainia, M., White, M.L., 2013. The use of alkali
635 activated waste binders in enhancing the mechanical properties and durability of soft
636 alluvial soils. Eng. Geol. 152, 96–108.
637
638 [24] Zhang, M., Guo, H., El-Korchi, T., Zhang, G., Tao, M., 2013. Experimental
639 feasibility study of geopolymer as the next-generation soil stabilizer. Constr. Build.
640 Mater. 47, 1468–1478.
641
642 [25] Silva, R.A., Oliveira, D.V., Miranda, T., Cristelo, N., Escobar, M.C., Soares, E.,
643 2013. Rammed earth construction with granitic residual soils: The case study of northern
644 Portugal. Constr. Build. Mater. 47, 181–191.
645
646 [26] Buchwald, A., Kaps, C., Hohmann, M., 2003. Alkali-activated binders and pozzolan
647 cement binders–complete binder reaction or two sides of the same story, in: Proceedings
648 of the 11th International Conference on the Chemistry of Cement. Portland Cement
649 Association Durban, South Africa, pp. 1238–1246.
650
651 [27] Shi, C., Krivenko, P.V., Roy, D.M., 2006. Alkali-activated cements and concretes.
652 Taylor & Francis, London ; New York.
653
654 [28] Sukmak, P., Horpibulsuk, S., Shen, S-L., Chindaprasirt, P., Suksiripattanapong, C.
655 2013. Factors influencing strength development in clay-fly ash geopolymer, Constr.
656 Build. Mater., 47, 1125-1136.
657
658 [29] Sukmak, P., De Silva, P., Horpibulsuk, S., Chindaprasirt, P. 2015. Sulphate
659 resistance of clay-Portland cement and clay-high calcium fly ash geopolymer, J. Mater.
660 Civ. Eng., Vol. 27, No. 5, 04014158.
661 [30] Snellings, R., Mertens, G., Elsen, J., 2012. Supplementary Cementitious Materials.
662 Rev. Mineral. Geochem. 74, 211–278.
663
664 [31] Newman, E.S. 1941. Behaviour of calcium sulfate at high temperatures. J. of Res. of
665 Nat. Bur. of Stand., Vol 27, 191-196.
666
667 [32] Stern, K. H., and Weise, E. L. 1966. High temperature properties and decomposition
668 of Inorganic salts – Part 1 – Sulfates. National Standard Reference Data Series- National
669 Bureau of Standards 7, Issued October 1, 52p.
670
671 [33] Pop S-F., Ion, R.M. 2013. Thermal analysis of the chemical weathering of chalk
672 stone materials. J. of Optoelect. And Adv. Mat., Vol 15, No. 7- 8, 888 – 892.

673 [34] Cong, X., Kirkpatrick, R.J., 1996. 29Si MAS NMR study of the structure of calcium
674 silicate hydrate. Adv. Cem. Based Mater. 3, 144–156.
675
676 [35] Andersen, M.D., Jakobsen, H.J., Skibsted, J., 2003. Incorporation of Aluminum in
677 Calcium Silicate Hydrate (C−S−H) of Hydrated Portland Cements: A High-Field ^{27} Al
678 and ^{29} Si MAS NMR Investigation. Inorg. Chem. 42, 2280–2287.
679
680 [36] Sun, G.K., Young, J.F., Kirkpatrick, R.J., 2006. The role of Al in C–S–H: NMR,
681 XRD, and compositional results for precipitated samples. Cem. Concr. Res. 36, 18–29.
682
683 [37] Pardal, X., Brunet, F., Charpentier, T., Pochard, I., Nonat, A., 2012. ^{27} Al and ^{29} Si
684 Solid-State NMR Characterization of Calcium-Aluminosilicate-Hydrate. Inorg. Chem.
685 51, 1827–1836.
686
687 [38] Wilson M.J., 1994. Clay mineralogy: spectroscopic and chemical determinative
688 methods, Springer Science + Business Media.
689
690 [39] Knapik K, 2016. Experimental and numerical analyses of fly ash from fluidized bed
691 combustion applications for selected ground improvement. The Silesian University of
692 Technology, PhD thesis, 217p.
693
694 [40] Tajuelo Rodriguez, E., Garbev, K., Merz, 650 D., Black, L., Richardson, I.G., 2017.
695 Thermal stability of C-S-H phases and applicability of Richardson and Groves' and
696 Richardson C-(A)-S-H(I) models to synthetic C-S-H. Cem. Concr. Res. 93, 45–56.
697
698 [41] Provis John L., van Deventer Jannie S.J., 2009. Geopolymers Structure, processing,
699 properties and industrial applications, Woodhead Publishing in materials. Woodhead,
700 Cambridge.
701
702 [42] Occhipinti R., Tarantino S. C., Riccardi M. P., Sturini M., Speltini A., Maraschi F.,
703 Elmaleh A., Zema M., 2017. Alkali activation of sulfate-bearing kaolin. Proceedings of
704 the 16th International Clay Conference, Granada, Spain.
705